This manuscript has been published by the Journal of Structural Engineering 2019, Vol. 145(8), pp. 04019079
DOI: 10.1061/(ASCE)ST.1943-541X.0002368

Experimental Assessment of Bolted Moment End-plate Connections

Chen Zhu[1], Kim J. R. Rasmussen[2]; Shen Yan[3]; and Hao Zhang[4]

[1] PhD student, School of Civil Engineering, University of Sydney, Sydney NSW 2006, Australia. E-mail: czhu7452@uni.sydney.edu.au

[2] Professor, School of Civil Engineering, University of Sydney, Sydney NSW 2006, Australia. E-mail: kim.rasmussen@sydney.edu.au

[3] Postdoctoral Research Associate, School of Civil Engineering, University of Sydney, Sydney NSW 2006, Australia. E-mail: shen.yan@sydney.edu.au

4 Associate Professor, School of Civil Engineering, University of Sydney, Sydney NSW 2006, Australia. E-mail: hao.zhang@sydney.edu.au

ABSTRACT

The paper summarizes experiments recently conducted at the University of Sydney on bolted moment end-plate connections. The overall context of this work is to obtain full-range moment-rotation curves of the connections which can be used to validate analytical and numerical models. The full-range moment-rotation curve covers not only the elastic and inelastic ranges but also the post-ultimate and post-fracture ranges. Thirteen specimens were tested with failure modes being either end-plate bending failure or column web buckling failure. Results of all experiments are provided in detail, including the full-range moment-rotation curves, observations of the two failure modes and deformations of individual joint components. The ultimate resistance of the bending tests are compared with those predicted by the AISC design guide and Eurocode3 Part 1.8 specification.

Introduction

It is well-known that semi-rigidity of joints can severely affect the strength and serviceability of unbraced steel frames. Therefore, a large number of studies have been carried out to investigate the semi-rigid responses of different types of beam-to-column joints (Bursi and Jaspart 1998; de Lima et al. 2004; Girão Coelho et al. 2004; Simões da Silva et al. 2004; Cabrero and Bayo 2007; Grimsmo et al. 2015; Dai et al. 2018). Based on these studies, many approaches have been proposed aiming at accounting for the inelastic response of joints under a variety of loading scenarios (Kishi and Chen 1990, Simões da Silva et al. 2000, Del Savio et al. 2009). Research on connections is now mature as far as initial semi-rigid stiffness and ultimate capacity are concerned, and has been

This manuscript has been published by the Journal of Structural Engineering 2019, Vol. 145(8), pp. 04019079
DOI: 10.1061/(ASCE)ST.1943-541X.0002368

incorporated into a consistent design framework in Part 1.8 of Eurocode3 which is based on the Component Method (Weynand et al. 1996; CEN 2010). Eurocode3 also includes provisions for determining the inelastic transition from the initial linear range to the ultimate capacity.

Studies on the post-ultimate response of joint are comparatively few. However, the post-ultimate performance of joints is also of significant importance in structural analysis and design for the following reasons. Firstly, a joint can sustain a considerable deformation in the post-ultimate range, and thus can absorb large amounts of energy, provided the joint is designed to possess good deformation capability before final failure. Secondly, the deformation capacity of joints is important because progressive collapse analyses are becoming increasingly common in practice, and these require the deformation capacity of joints and members under large displacements (Izzuddin et al. 2008; Vlassis et al. 2008). Thirdly, advances in computing power and analysis software over the last decade have made it possible to design steel structural frames by computer without recourse to a structural standard for individual member and joint checks (Zhang et al., 2016a; Zhang et al., 2016b). In this design-by-analysis approach, the actual nonlinear full-range behaviour of joints is required such that the strength and structural safety checks can be performed in a single step at system level. For these reasons, the post-ultimate response of joints has drawn increasing attention among the engineering community recently. For example, a component model using tri-linear springs has been proposed for modelling the full-range response of joints (Lewis 2010). Physical tests are indispensable in validating such models. Unfortunately, few experiments considering the post-ultimate response of beam-to-column connections have been reported. This paper presents an experimental program specifically aimed at obtaining the full-range moment-rotation response of a series of bolted moment end-plate connections.

For bolted moment end-plate connections, one of the main components contributing to the joint rotation is end-plate bending. The end-plate bending causes severe deformation at the extended part of the end-plate, leading to the crack initiation propagation adjacent to the welds connecting the end-plate to the flange of the beam. Crack propagation manifests itself as stages of abrupt reductions in resistance, as seen in several tests (Cabrero and Bayo 2007; Girão Coelho et al. 2004). Column web buckling is another main component contributing to the joint rotation in end-plate connections with unstiffened column webs, and is a potential failure mode as recorded in early tests (Chen and Oppenheim 1970). In practice, this failure mode is usually avoided by introducing web stiffeners. Although web plate buckling may reduce the moment capacity, it presents a ductile mode of failure with significant rotation capacity. However, there is limited knowledge of the full-range column web buckling behaviour.

A total of 13 bolted moment end-plate connections with unstiffened column webs are tested in this study. The tested connections are loaded far into the post-ultimate range, and two failure modes are expected, i.e., end-plate bending failure and column web buckling failure. Two joint configurations are examined with four different loading conditions applied, including major-axis bending, combined bending and axial force, minor-axis bending and bi-axial bending. Full-range moment-rotation responses of all tested connections are recorded throughout the experiments, as are the deformations of the end-plates and column webs.

Experimental program

General

Table 1 presents a summary of the 13 tests in this experimental program, and Fig. 1 shows the dimensions of the connections. Only a single geometric parameter was varied, namely the thickness of the end-plate, so that the failure modes and loads could be readily compared. The connections with a 10 mm thick end-plate were expected to fail in the end-plate bending mode, while those with 20 mm end-plates, all strengthened by backing plates to effectively prevent the end-plate from deforming at the tension face, were expected to fail in the column web buckling mode. All four loading conditions were applied on both types of connections. One of the 10 mm end-plate connections (No. 2 in Table 1) had a backing plate, in order to investigate the effect of backing plates on the end-plate bending mode. All other 10 mm end-plate connections did not have backing plates.

Specimen details

All specimens were manufactured from AS 350 grade steels to AS/NZS 3679.1 (2010), and used the same beam-column combination of 310UB 46.2 beam and 310UC 96.8 column. Table 2 shows the mechanical properties of the specimen materials, which were obtained through coupon tests in accordance with the AS 1391 (2017). The length of the column was 1200 mm between the centers of the pinned supports, and the length of the beam was 1000 mm between the end-plate and the loading point. The lengths of the beam and the column were consistent with those chosen for similar tests described in literature (de Lima et al. 2004). For this length of beam, the curvature caused by bending was insignificant, so was the effective shear action on the connection compared to the bending action.

The end-plate was welded to one end of the beam using full strength 45˚continuous fillet welds. The welding procedure was manual metal arc welding using E48/W50X welding rods with a nominal tensile strength of 480MPa. The end-plate was bolted to a column flange using six M24 grade 8.8 high tensile bolts, the strength of

which was sufficient to transmit the applied loads from the end-plate to the column flanges up to and beyond the ultimate connection capacity, such that the tensile bolts would not be the first component to fail. The arrangement of the bolts was determined according to the ASI Connection Design Guide (Hogan 2009), as shown in Fig. 1.

Test setup

Figure 2 shows the test setup. The rig was constructed with several movable parts and thus could accommodate different test setups. The column ends were connected to the supports using pins, with one end fixed against displacements while the other end capable of moving horizontally, ensuring simply supported conditions at the column ends. The supports were attached to the strong floor and was sufficiently stiff to resist any noticeable deformation. The end of the beam was loaded using a servo-controlled hydraulic jack with 1000kN loading capacity and 250mm travel distance. The hydraulic jack was installed on a reaction frame, adjustable in height to accommodate different loading conditions. The reaction frame was available from previous test programs. It was bolted to the strong floor and could resist up to 360kN of lateral loading without any noticeable deformation. Moreover, the specimens were restrained laterally by two braces placed at the mid-to-upper part of the beam to prevent out-of-plane displacement. The contact planes between the braces and the specimen were filled with Teflon plates to minimize friction.

Figure 2a shows the test setup of the major-axis bending tests (Nos 1, 2 and 8 in Table 1). The column was in a horizontal position, and thus the beam was in a vertical position and perpendicular to the loading arm. The major action on the connection was in-plane bending.

Figure 2b shows the test setup of the combined bending and axial tension force tests (Nos 3, 4 in Table 1), and Fig. 2c shows that of the combined bending and axial compression force tests (Nos 9 and 10 in Table 1). For all tests, one end of the column was lifted to a predefined height using a column support extension to introduce an angle (θ_1) between the loading direction and the direction perpendicular to the axis of the beam. A larger angle created a larger axial force in the connection, and therefore two angles were considered, namely, 19° and 34°. The tests with 19° tilting angle were referred as the small axial load tests while those with 34° tilting angle were referred as the large axial load tests, as shown in Table 1. To increase, rather than decrease, the likelihood of connection failure, the connections with a 10 mm thick end-plate expected to fail due to end-plate bending were loaded with the combined actions of bending and axial tension. In contrast, the connections with a 20 mm thick end-plate expected to experience column web buckling failure were loaded with the combined actions of bending and axial compression.

Figure 2d shows the test setup of the minor-axis bending tests (Nos 7 and 13 in Table 1). Compared with the major-axis bending tests, each specimen in this category was rotated 90° about the centerline of the beam. Thus, the loading direction was perpendicular to the minor axis of the beam. The major action on the connection was bending about the minor axis.

Figure 2e shows the setup of the bi-axial bending tests (Nos 5, 6, 11 and 12 in Table 1). Major-axis bending and minor-axis bending were applied to the connection simultaneously, while keeping the ratio between the bending moments during the test. The bi-axial bending action was achieved by rotating the specimen about the centerline of the beam to create an angle (θ_2) between the loading direction and the major axis bending plane of the beam. A larger angle created larger minor-axis bending moment. Two angles were considered, i.e., 11° or 24°. Tests with the angle of 11° were referred as bi-axial bending tests with small minor-axis bending while those with the angle of 24° were referred as bi-axial bending tests with large minor-axis bending, as shown in Table 1. The beam was restrained by lateral bracing members in order to move in the loading direction of the jack.

Instrumentation

All tests were instrumented as illustrated in Fig. 3, with displacement transducers and an inclinometer. All data were recorded at 1 sec intervals.

The applied moment and the connection rotation are calculated based on measurements of the load cell in the hydraulic jack, displacement transducer DT1 and inclinometer. During the tests, DT1 was constantly changed to be perpendicular to the beam to keep the measured displacement increment ($\Delta\delta$) perpendicular to the beam. For every second, the increment of the total rotation of the beam ($\Delta\theta_{\mathrm{t}}$) and the real-time total rotation (θ_{t}) can be obtained by

$$\Delta\theta_{\mathrm{t}} = \mathrm{atan}\left(\frac{\Delta\delta}{L}\right) \tag{1}$$

$$\theta_{\mathrm{t}} = \sum \Delta\theta_{\mathrm{t}} \tag{2}$$

where L is the length of the beam.

The applied load perpendicular to the beam (P) and the resulting applied moment (M) can be then calculated by

$$P = \cos(\theta_1 + \theta_{\mathrm{t}} - \theta_{\mathrm{LA}}) \cdot \cos\theta_2 \cdot P_{\mathrm{LC}} \tag{3}$$

$$M = PL \tag{4}$$

where P_{LC} is the measurement of the load cell, θ_{LA} is the rotation of the loading arms measured by the inclinometer, θ_1 and θ_2 are the loading-associated angles as defined in Table 1.

The total rotation of the beam θ_{t} includes the beam rotation (θ_{d}) caused by beam bending deflection, and therefore the connection rotation (θ) is calculated by subtracting θ_{d} from θ_{t}, i.e.,

$$\theta = \theta_t - \theta_{\mathrm{d}} = \theta_t - \mathrm{atan}(\frac{PL^2}{3EI}) \quad (5)$$

where θ_{d} is calculated according to the engineering beam theory, E is the Young's modulus and I is the second moment of area of the beam.

The key components of the extended end-plate connections investigated in this experimental program include the end-plate bending component and the column web buckling component. For the end-plate bending component, the applied force (P_{epb}) is the force transmitted by the flange on the tension face, the magnitude of which can be approximately calculated as

$$P_{\mathrm{epb}} = \frac{M}{z} + 0.4 \cdot \sin(\theta_1 + \theta_{\mathrm{t}} - \theta_{\mathrm{LA}}) \cdot \cos\theta_2 \cdot P_{\mathrm{LC}} \quad (6)$$

where z is the distance between the centers of the beam flanges, and the factor of 0.4 was adopted because the area of the tensile flange was about 40% of the total area of the entire beam cross-section. The deformation (Δ_{epb}) was obtained as the difference between readings of two displacement transducers (DT2 and DT3) on the end-plate,

$$\Delta_{\mathrm{epb}} = \delta_{\mathrm{DT2}} - \delta_{\mathrm{DT3}} \quad (7)$$

For the column web buckling component, the applied force (P_{cwc}) is the force transmitted by the flange on the compression face, and thus can be approximately calculated according to

$$P_{\mathrm{cwc}} = \frac{M}{z} - 0.4 \cdot \sin(\theta_1 + \theta_{\mathrm{t}} - \theta_{\mathrm{LA}}) \cdot \cos\theta_2 \cdot P_{\mathrm{LC}} \quad (8)$$

The deformation (Δ_{cwc}), taken as the vertical shortening of the column web, was obtained as the difference between readings of the two displacement transducers DT4 and DT5,

$$\Delta_{\mathrm{cwc}} = \delta_{\mathrm{DT4}} - \delta_{\mathrm{DT5}} \quad (9)$$

Test procedure and raw data processing

All specimens were tested following the same loading procedure, commencing after a specimen was in position and all instrumentation was installed and connected. The displacement rate was set at 1 mm/sec. Every 10-20 minutes, the test was stopped for 2 minutes to acquire the static resistance. Since the stroke of the hydraulic jack was limited to 200mm, the loading arrangement had to be reset after every 150mm of extension using new holes in the loading arms. This required the specimen to be unloaded and reloaded after resetting the loading arrangement. Finally, after the resistance decreased to less than 25% of the ultimate resistance, the test was terminated.

The raw data were processed to acquire smooth continuous curves of static resistance. A sample moment-rotation curve is shown in Fig. 4. The static resistance was the same as the quasi-static (dynamic) resistance in the elastic range, but in the inelastic range was approximately 3% lower than the quasi-static resistance as a result of the stress relaxation. In the late loading range where fracture occurred, the static resistance was assumed to be 3% lower than the quasi-static resistance.

Connection Behaviour

Major-axis bending tests

The major-axis bending tests included tests of S10, S10BP and S20BP (see Table 1). Their moment-rotation curves as well as the failure modes are shown in Fig. 5.

For test S10, the ultimate bending moment was 212 kN·m, with a corresponding rotation of 0.119 rad. Before reaching the ultimate resistance, two cracks had emerged in the heat affected zone (HAZ) of the welds, facing the two bolts in the extended part of the end-plate. In the post-ultimate range, the bending strength was reduced in several stages. When the connection had just passed its ultimate resistance, the two initial cracks grew wider and merged together. This coalescence of cracks caused the first drop in resistance. The merged crack grew around the tip of the flange on one side, and towards the edge of the end-plate on the other side. Eventually the propagated crack caused the extended part of the end-plate to tear off the connection. This tear resulted in the second drop in resistance. Subsequently, the crack propagation continued in the HAZ along the inside tension flange and eventually along the web plate, which increased the tension forces in the bolts on the tension side and finally caused one bolt to break. This coincided with the third abrupt drop in resistance on the moment-rotation curve, leading to the complete failure of the connection.

Specimen S10BP had higher stiffness than specimen S10. This was because the backing plates prevented the column flange of S10BP from yielding and thus reduced its flexibility compared to S10. Moreover, S10BP also gained a slight increase in strength to 218 kN·m due to the installation of the backing plate. However, its corresponding rotation was reduced to 0.107 rad, which was 10% less than that of S10. In the post-ultimate range, the bending strength of S10BP experienced similar abrupt reductions as S10 due to sequential failures of connection components. Unlike the S10 test, one side of the beam flange was observed to be pulled off from the end-plate during the fracture propagation in the HAZ along the tension flange.

S20BP had 20mm thick end-plates and backing plates which greatly strengthened its performance in the tension zone. Consequently, S20BP failed in the compression zone due to column web buckling, and the ultimate

bending resistance was 293 kN·m. Both the ultimate strength and the corresponding rotation were significantly higher than those of S10 and S10BP. In the post-ultimate range, the joint strength reduced smoothly as the column web deflection gradually increased until S20BP completely failed due to the fractures of the tensile bolts at the outer bolt row. From a strength and ductility point of view, S20BP performed significantly better than the S10 and S10BP connections with 10 mm thick end-plates.

Major-axis bending with axial force tests

Four tests were carried out with both major-axis bending and axial loading applied to the connections, viz., S10_TS, S10_TL, S20BP_CS and S20BP_LT (see Table 1). The measured moment-rotation curves and failure modes are shown in Fig. 6 and Fig. 7.

S10_TS and S10_TL were loaded under both bending and axial tension, and had similar end-plate bending failure modes. The connection failures were characterized by the growth of a crack in the HAZ along the tension flange, the extension of the crack to the edge of the end-plate, the pull-off of the tension beam flange and bolt fracture. This was similar to the S10 connection subjected to bending only, and therefore the additional axial tension load did not change the failure mode of end-plate connections failing in the end-plate bending failure mode. However, the gradual yielding range of the connections with additional axial tension load were lower than that of S10. The ultimate bending resistances of S10_TS and S10_TL were reduced by 5.2% and 12.0%, respectively. Hence, the axial tension force had an appreciable influence on the load-carrying ability of end-plate connections failing in the end-plate bending failure mode.

For the loading scheme adopted in the tests, the axial force increased along with the applied bending moment. When the connections reached their ultimate bending resistances, the applied axial tension in test S10_TS and S10_TL were 88 kN and 140 kN, respectively. The axial plastic resistance of the beam is 2095 kN, so the above maximum applied tension forces accounted for 4.2% and 6.7% of the beam's axial plastic resistance, respectively. Eurocode3 suggests that the axial load may be disregarded when its value is less than 5% of the beam's axial plastic resistance. This was not consistent with test S10_TS which showed that an axial force of 4.2% of the plastic resistance can cause a reduction of 5.2% of the connection bending resistance. Moreover, the test S10_TL illustrated that the bending resistance reduction (of 12.0% for this specimen) due to axial tension force (of 6.7% of the plastic resistance) was increasing in a nonlinear fashion.

Specimen S20BP_CS and S20BP_CL were loaded under combined bending and axial compression. Both connections failed due to column web buckling, similar to the S20BP connection. However, the compressive axial

load precipitated the column web buckling, and therefore both connections reached their ultimate bending resistance significantly earlier than S20BP. The ultimate bending resistances of S20BP_CS and S20BP_LT were reduced by 12.1% and 15.1%, respectively, compared with that of S20BP loaded with bending action only. At the ultimate resistance state, the applied axial compressive forces in tests S20BP_CS and S20BP_LT were 66 kN and 138 kN, respectively, which accounted for 3.2% and 6.6% of the beam's axial plastic resistance. Therefore, for end-plate connection with a column buckling failure mode, the detrimental influence of additional axial compressive load is more severe than impliedly Eurocode3, which allows the effect to be ignored when the axial load is less than 5% of the beam's axial plastic resistance as previously mentioned. Thus, there is a clear need to investigate the effect of axial force on bolted moment end-plate connections and to develop a mechanical model accounting for the effect of axial forces, especially for unstiffened web connections subjected to compressive axial forces.

The post-ultimate behaviours of S20BP_CS and S20BP_CL were different from that of S20BP, as illustrated by the different shapes of the moment-rotation curves. In the S20BP_CS test, a crack formed in the HAZ along the tension flange but did not spread to the edge of the end-plate within the deformation range of the test. The connection preserved 60% of the ultimate bending resistance when the rotation reached 0.49 rad. In the S20BP_CL test, no component failed on the tension side, and thus the post-ultimate resistance showed an even more gradual reduction that the S20BP_CS test.

Bi-axial bending tests

Four tests were carried out with bi-axial bending applied on the connections, viz., S10_BS, S10_BL, S20BP_BS and S20BP_BL (see Table 1). The moment-rotation curves and failure modes are shown in Fig. 8 and Fig. 9.

For the connections with a 10 mm thick end-plate (S10_BS and S10BL) failing in the end-plate bending failure mode, the additional out-of-plane bending induced by the minor-axis moment affected both the initial stiffness and the gradual yielding range, leading to lower moment-rotation curves over this range, as shown in Fig. 8. The ultimate major-axis bending resistance of S10_BL was 14.8% smaller than that of S10. However for S10_BS, the bending resistance was observed to be increased by 5.8%. The increase in strength may be caused by random variations introduced during fabrication, including better-than-expected welding quality in this case as illustrated by the failed components of the connection. For S10 and S10_BL, the initiation of cracks in the HAZ along the tensile beam flange gave rise to the first drops in the post-ultimate curves, which were followed by gradual pull-off of the beam flange from the end-plate. However, in test S10_BS this incipient crack did not occur, allowing

for continuous hardening in the bending strength until the pulling-off of the tensile beam flange caused the first drop in resistance.

In the post-ultimate region, unexpectedly high friction between the beam and the lateral bracing was observed due to a large deformation of the specimen. When component failure occurred on the tension side and was about to cause a sudden drop in resistance, the friction helped to provide a temporary resistance to the unbalanced force, such that the drops in the post-ultimate curves were not as abrupt as in test S10. S10_BL was affected more by the friction, and thus the drops in the post-ultimate region were not distinct at all. The friction started to resist the applied load from the hydraulic jack in the later stage of the post-ultimate range, and then the test was terminated.

S20BP_BS and S20BP_BL were subjected to bi-axial bending, and failed in the column web buckling mode as did other connections with a 20 mm thick end-plate. The additional minor-axis bending reduced the initial stiffness, the ultimate strength as well as the rotation corresponding to the ultimate major-axis bending moment, as shown in Fig. 9. It also changed the shapes of the moment-rotation curves in terms of more gradual yielding and less reduction in moment in the post-ultimate response. For both tests, friction between the beam and the lateral bracings was again observed in the post-ultimate range. The friction started to resist the load applied by the hydraulic jack in the later stage, and thus the tests were terminated. No component failure was observed on the tensile side of the connections.

Minor-axis bending tests

Two tests in this series were designed to assess the minor-axis performance of the end-plate connections. Figure 10 shows the moment-rotation curves and the deformed shape of a typical connection.

The connections had much smaller initial bending stiffness under minor-axis bending. S10_M and S20BP_M showed similar initial stiffness, which was about only 2.6% of the S10 connection and 2.4% of the S20BP connection. For both connections, the major source of deformation was the column flange twisting rather than end-plate bending, and therefore these two connections had similar post-yielding responses. The column flange twisting deformation capacity was observed to be extensive, and thus both connections did not reach their ultimate resistance in the tests.

The results of all tests are summarised in Table 3, including the faiure modes, the ultimate bending resistances along with the corresponding axial forces or the minor-axis bending moments, and the correspoding joint rotations.

Failure mechanism

End-plate bending failure

All connections with a 10 mm thick end-plate except for the one subjected to minor-axis bending (S10_M) failed in an end-plate bending failure mode. These connections showed very similar post-ultimate behaviours, featuring three major drops in the moment-rotation curve. Figure 11 shows a typical example of the failure process of the end-plate bending failure mode. Four stages can be used to describe the failure process, the last three of which gave rise to the three drops in the moment-rotation curves.

The first stage was very short and occurred when the bending resistance was about to reach its ultimate value. Two cracks started to emerge in the HAZ of the welds, facing the two bolts in the extended part of the end-plate. Because in this stage cracks existed only on the surface and were still very small and because of material hardening, the bending resistance of the connection did not drop abruptly.

In the second stage, the two initial cracks grew wider and coalesced until reaching the full width of the beam flange, causing the first drop in resistance. The connection preserved 71% to 77% of its ultimate bending strength after this drop. (S10–72%, S10BP–73%, S10_TS–71%, S10_TL–75%, S10_BS–77%; the first drop in test S10_BL was not very clear.)

In the third stage, the merged crack grew towards the edge of the end-plate on one side, and eventually caused the extended part of the end-plate to be torn apart, leading to the second drop in resistance. At this time, the load on the tension side of the end-plate was mainly transferred by the beam flange on the opposite side to the crack growth. Thus the crack usually also grew around the tip of the flange, and the beam flange on this side was pulled off from the end-plate. This phenomenon was more significant when there was minor-axis bending moment applied on the connection. At the end of this stage, the connection could preserve 41% to 45% of its ultimate bending resistance. (S10–43%, S10_BP–41%, S10_TS–45%, S10_BS–44%; the second drops in test S10_TL and S10_BL were not very clear.)

In the fourth and final stage, the outer bolt on the end-plate tearing side no longer transferred load, and thus the inner bolt on the same side had to carry increasing load, leading to its fracture eventually. At the same time, the crack around the beam flange tip would grow along the inner side of the beam flange, toward the beam web, and down along the beam web for a certain depth. The bolt failure and fracture propagation led to the complete failure of the connection, and appeared as the third abrupt drop on the moment-rotation curve. The remaining bending strength was below 40% of the ultimate strength. (S10–20%, S10BP–37%, S10_TS–36%, S10_TL–40%, S10_BS–26%; test S10_BL was terminated before the fourth stage.)

It was observed that all tested connections had very similar post-ultimate behaviours, in terms of both the sequence of fracture propagation and the moment-rotation curve. Therefore, it is possible to model the post-ultimate behaviour of an end-plate connection based on these three stages of post-ultimate response.

Column Web Buckling Failure

All connections with a 20 mm thick end-plate except for the one under minor-axis bending (S20BP_M) failed due to the buckling of the column web.

The web deformation grew slowly until the load approached the ultimate resistance, at which web buckling appeared. Thenceforth, the web buckling deformation grew quickly and the resistance reduced accordingly. In the pre-ultimate range, the connections were visibly affected by the different loading conditions, leading to different overall shapes of the moment-rotation curves as shown in Fig. 7 and Fig. 9. The additional axial force had limited influence on the initial stiffness, but reduced the ultimate major-axis bending resistance by a large margin. The additional minor-axis bending, however, caused significant reduction of both the initial stiffness and the ultimate major-axis bending resistance.

The bending resistance was reduced gradually in the post-ultimate range. Different loading conditions resulted in different rates of reduction, but all connections preserved over 70% of their ultimate strength under a large rotation up to 0.25 rad. The complete failure of the connection was caused by the fracture on the tension side, either tensile bolt fracture or crack propagation in the HAZ along the tension flange.

Component Behaviour

End-plate Bending Component

Figure12 shows the force versus displacement curves of the end-plate bending component. For the 10mm thick end-plates, the bending responses were stiff in the initial elastic range before gradually yielding. As observed from the curves, both the initial elastic stiffness and the ultimate strength were similar for all the tests. Hence, the backing plates and the axial forces had limited effects on the end-plate bending behaviour. The 20 mm thick end-plates had a substantially longer elastic range than the 10 mm thick end-plates, and the ultimate strength was also enhanced.

Column Web Buckling Component

Figure 13 shows the force versus displacement curves of the column web buckling component. The recorded column web behaviour was typical of stocky plate buckling in that it had almost infinite initial stiffness followed by positive inelastic post-buckling stiffness until it reached the ultimate resistance, and then negative post-ultimate stiffness. The 10 mm thick end-plate tests failed by end-plate bending, and consequently, the column web in these tests did not reach the ultimate strength and the buckled web deflection in those tests elastically unloaded when the applied load decreased in the post-ultimate range. Moreover, different loading conditions created different constraining effects on the column web plate, thus influencing the post-buckling strength of the column web. In the bi-axial bending tests and the minor-axis bending tests, the column top flanges twisted introducing a rotational displacement in addition to the column web shortening, which affected the readings of displacement transducer DT4. Consequently, the column web shortening responses of these tests are not presented here.

Comparison with Eurocode3 and AISC strength models

The strength of S10 and S20BP were obtained using Eurocode3 (CEN 2010) and the AISC design guide (Murray and Sumner 2003). The provisions of Eurocode3 are based on the component method, and allow for calculating the pre-ultimate behaviour of a connection, including the initial elastic behaviour, the gradual yielding curve and the ultimate bending resistance. The connection is assumed to maintain the ultimate bending resistance with the increasing joint rotation. The AISC design guide is based on the limit state method, and only contains provisions for calculating the ultimate moment of a joint.

The results from both methods are presented in Fig. 14 in terms of moment-rotation curves, and in Table4 showing the ultimate bending resistance and the initial stiffness. Eurocode3 consistently underestimates the ultimate moment by 33%~38%, while the AISC design guide underestimates the strength of S10 and S20BP by 50% and 13%, respectively.

Conclusions

An experimental investigation is presented in this paper on bolted moment end-plate connections subjected to four different loading conditions, including major and minor axis bending, bi-axial bending and combined bending and axial force. Particular attention was paid to obtaining the full-range behaviour of the joints including the post-ultimate range. The paper presents moment-rotation curves, and explains the failure sequence of the joints including fracture propagation. Force-displacement curves were also presented for two joint components, namely, the extended end-plate and column web plate.

The moment-rotation curve of the end-plate connection was found to be considerably affected by the failure mode, especially in the post-ultimate range. Those connections failing by end-plate bending had three distinct drops in resistance in the post-ultimate range at around similar levels of resistance. Each abrupt drop in resistance was associated with the fracture of welds or bolts. Conversely, tests failing by column web buckling had an extensive gradual post-ultimate curve that eventually dropped abruptly due to bolt fracture.

The additional axial load and minor-axis bending had noticeable effects on the connection behaviour. While the additional axial force had little influence on the initial stiffness, it reduced the ultimate major-axis bending resistance by a large margin. The additional minor-axis bending caused significant reduction of both the initial stiffness and the ultimate major-axis bending resistance.

The dimensions of individual components had a significant impact on the connection behaviour in that two distinct failure modes were achieved by changing the thickness of the end-plate. Consequently, the performance of each component is important in the design of bolted moment end plate connections. The paper presents load-deflection curves for the extended end plate component and load-shortening curves for the column web plate, as obtained from the joint tests.

The ultimate moment capacities of the joints subject to major axis bending are compared to design moments predicted by Eurocode3 and AISC guidelines. Both methods underestimate the ultimate moment of two selected tests by more than 30% except the AISC model for S20BP which is only 13% smaller than the experimental ultimate moment.

References

AS/NZS 3679.1 (2010). “Structural steel Part 1: Hot-rolled bars and sections.” Standards Australia., Sydney, Australia.

AS 1391 (2017). “Metallic materials - Tensile testing at ambient temperature.” Standards Australia., Sydney, Australia.

Bursi, O. S. and Jaspart, J. P. (1998). "Basic issues in the finite element simulation of extended end plate connections." Computers & Structures, 69 (3), 361-382.

Cabrero, J. M., and Bayo, E. (2007). "The semi-rigid behaviour of three-dimensional steel beam-to-column joints subjected to proportional loading. Part I. Experimental evaluation." Journal of Constructional Steel Research, 63 (9), 1241-1253.

CEN (European Committee for Standardization). (2010). “EN 1993-1-8, Eurocode3: design of steel structures, Part 1-8: design of joints”, European Committee for Standardization, Brussels.

Chen, W. F. and Oppenheim, I. J. (1970). Web buckling strength of beam-to-column connections, Fritz Engineering Laboratory Report, No.333.

Dai, L., Zhao, X., and Rasmussen, K. J. R. (2018). “Flexural behaviour of steel storage rack beam-to-upright bolted connections”. Thin-Walled Structures, 124, 202-217.

de Lima, L. R. O., Simões da Silva, L., da S. Vellasco, P. C. G., and de Andrade, S. A. L. (2004). "Experimental evaluation of extended endplate beam-to-column joints subjected to bending and axial force." Engineering Structures, 26 (10), 1333-1347.

Del Savio, A. A., Nethercot, D. A., Vellasco, P. C. G. S., Andrade, S. A. L. and Martha, L. F. (2009). "Generalised component-based model for beam-to-column connections including axial versus moment interaction." Journal of Constructional Steel Research, 65 (8), 1876-1895.

Girão Coelho, A. M., Bijlaard, F. S. K., Gresnigt, N. and Simões Da Silva, L. (2004). "Experimental assessment of the behaviour of bolted T-stub connections made up of welded plates." Journal of Constructional Steel Research, 60 (2), 269-311.

Grimsmo, E. L., Clausen, A. H., Langseth, M. and Aalberg, A. (2015). "An experimental study of static and dynamic behaviour of bolted end-plate joints of steel." International Journal of Impact Engineering, 85 (Suppl. C), 132-145.

Hogan, T. J. (2009). Connection Design Guide 12 - Bolted end-plate to column moment connections. Australian Steel Institute Connection Design Guide. Australian Steel Institute (ASI), Sydney.

Izzuddin, B. A., Vlassis, A. G., Elghazouli, A. Y. and Nethercot, D. A. (2008). "Progressive collapse of multi-storey buildings due to sudden column loss - Part I: Simplified assessment framework." Engineering Structures, 30 (5), 1308-1318.

Kishi, N. and Chen, W. F. (1990). "Moment‐Rotation Relations of Semirigid Connections with Angles." Journal of Structural Engineering, 116 (7), 1813-1834.

Lewis, K. (2010). The component method of joints, Master’s thesis, School of Civil Engineering, University of Sydney, Sydney, Australia.

Murray T. M. and Sumner E. A. (2003). *Design Guide 4: Extended End-plate Monent Connections Seismic and Wind Applications*. American Institute of Steel Construction.

Simões da Silva, L., Coelho, A. G. and Lucena Neto, E. (2000). "Equivalent post-buckling models for the flexural behaviour of steel connections." Computers & Structures, 77 (6), 615-624.

Simões da Silva, L., de Lima, L. R. O., da S. Vellasco, P. C. G. and de Andrade, S. A. L. (2004). "Behaviour of flush end-plate beam-to-column joints under bending and axial force." Steel and Composite Structures, 2 (4), 77-94.

Vlassis, A. G., Izzuddin, B. A., Elghazouli, A. Y. and Nethercot, D. A. (2008). "Progressive collapse of multi-storey buildings due to sudden column loss - Part II: Application." Engineering Structures, 30 (5), 1424-1438.

Weynand, K., Jaspart, J. P., and Steenhuis, M. (1996) "The stiffness model of revised annex J of Eurocode3", in: R. Bjorhovde, A Colson, R Zandonini (Eds.), Connections in steel structures III". Proceedings of the 3rd Int.Workshop on Connections, Elsevier, Trento, 441–452.

Zhang, H., Shayan, S., Rasmussen, K. J. R. and Ellingwood, B. R. (2016). "System-based design of planar steel frames, I: Reliability framework." Journal of Constructional Steel Research, 123, 135-143.

Zhang, H., Shayan, S., Rasmussen, K. J. R. and Ellingwood, B. R. (2016). "System-based design of planar steel frames, II: Reliability results and design recommendations." Journal of Constructional Steel Research, 123, 154-161.

Zhu, C., Rasmussen, K. J. R. and Yan, S. (2018). "Component model for column webs in compression." Thin-walled Structures. (Submitted for publication.)

Tables

Table 1 Summary of studies of connections

No.	Name	End-plate	Backing plate	Loading condition		
				Description	θ_1	θ_2
1	S10	10mm	No	major-axis bending	0	0
2	S10BP	10mm	Yes	major-axis bending	0	0
3	S10_TS	10mm	No	major-axis bending with **T**ension **(S**mall)	19	0
4	S10_TL	10mm	No	major-axis bending with **T**ension (**L**arge)	34	0
5	S10_BS	10mm	No	**B**i-axial bending (**S**mall minor-axis bending)	0	11
6	S10_BL	10mm	No	**B**i-axial bending (**L**arge minor-axis bending)	0	24
7	S10_M	10mm	No	**M**inor-axis bending	0	90
8	S20BP	20mm	Yes	major-axis bending	0	0
9	S20BP_CS	20mm	Yes	major-axis bending with **C**ompression (**S**mall)	-19	0
10	S20BP_CL	20mm	Yes	major-axis bending with **C**ompression (**L**arge)	-34	0
11	S20BP_BS	20mm	Yes	**B**i-axial bending (**S**mall minor-axis bending)	0	11
12	S20BP_BL	20mm	Yes	**B**i-axial bending (**L**arge minor-axis bending)	0	24
13	S20BP_M	20mm	Yes	**M**inor-axis bending	0	90

Note: θ_1 is the angle between the loading direction and the transverse axis of the beam; θ_2 is the angle between the loading plane and the major bending plane of the beam, as shown in Fig. 2.

Table 2. Mechanical properties of specimens

	Yield stress (MPa)	Ultimate tensile strength (MPa)	Total Elongation (%)
Beam	353	505	26.3
Column	382	498	30.5
End-plate (10 mm)	425	567	24.5
End-plate (20 mm)	355	503	26.1

Table 3 Summary of testing results

Name	Failure mode	Ultimate resistance			Joint rotation at ultimate resistance (rad)
		Bending moment (kN·m)	Axial force (kN)	Minor-axis moment (kN·m)	
S10	EPB	212	–	–	0.119
S10BP	EPB	218	–	–	0.107
S10_TS	EPB	202	88	–	0.122
S10_TL	EPB	188	140	–	0.114
S10_BS	EPB	225	–	44	0.161
S10_BL	EPB	181	–	81	0.112
S10_M	–	–	–	–	–
S20BP	CWB	293	–	–	0.166
S20BP_CS	CWB	258	-66	–	0.089
S20BP_CL	CWB	249	-138	–	0.077
S20BP_BS	CWB	241	–	47	0.108
S20BP_BL	CWB	224	–	100	0.123
S20BP_M	–	–	–	–	–

Note: Failure mode: EBF – End-plate bending failure, CWB – Column web buckling failure; Axial force – positive value indicates tension, negative value indicates compression.

Table 4 Ultimate bending resistance and initial stiffness according to Eurocode3 and AISC Design Guide

Specimen	Ultimate bending resistance (kN·m)			Initial stiffness(kN·m/rad)	
	Test	Eurocode 3	AISC	Test	Eurocode 3
S10	217	133	108	8790	19500
S20BP	296	197	258	10500	22700

Figures

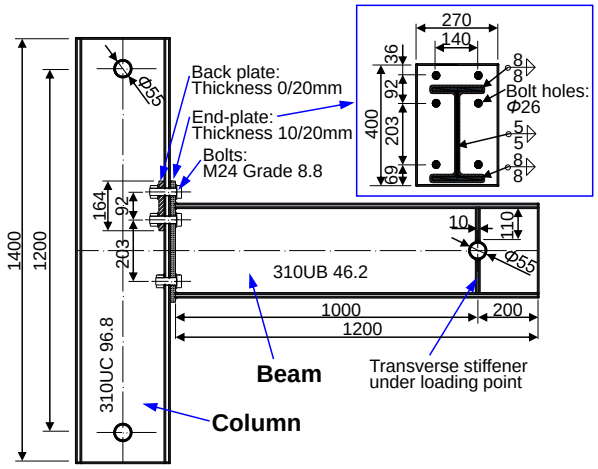

Fig. 1. Geometry of specimens

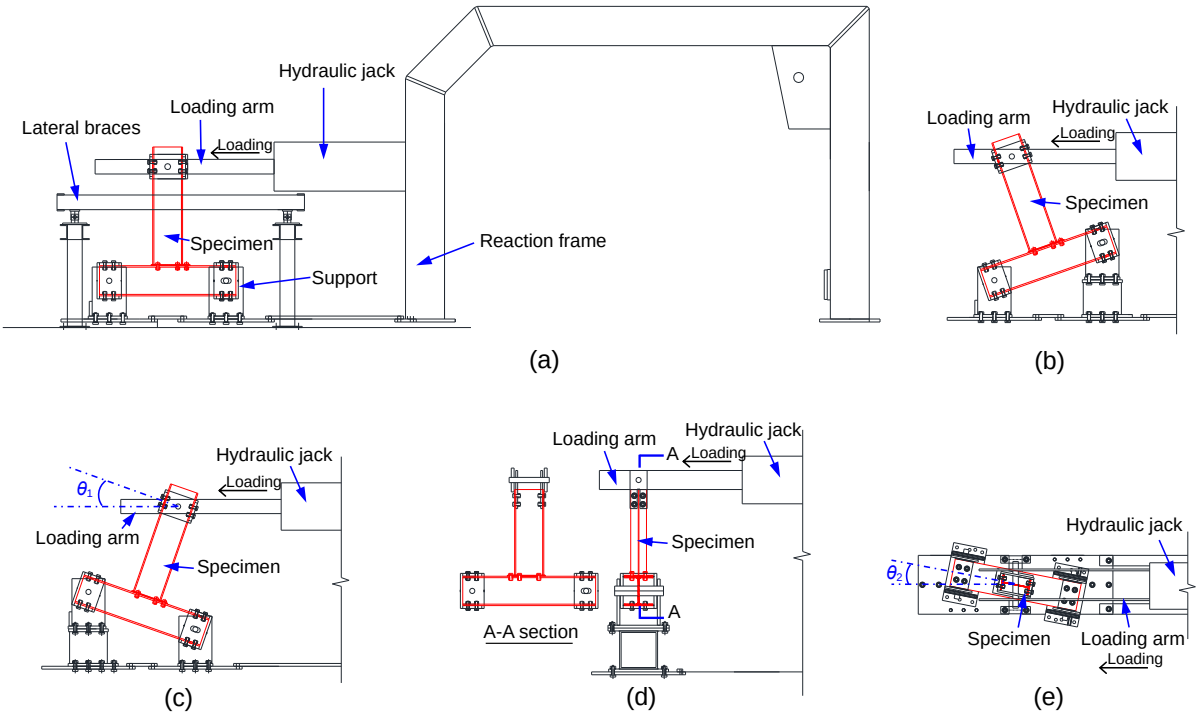

Fig. 2. Test Setup. (a) Major-axis bending tests; (b) major-axis bending with tension tests; (c) major-axis bending with compression tests; (d) minor-aixs bending test; (e) bi-axial bending tests. (Note: lateral restraint is not shown in figures (b)-(e); figure (e) shows a plan view)

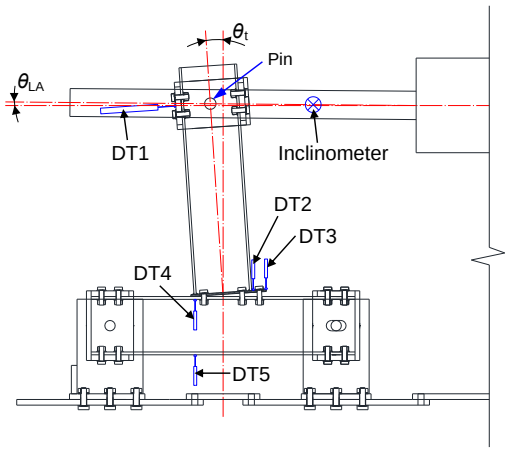

Fig. 3. Measurements of deformations

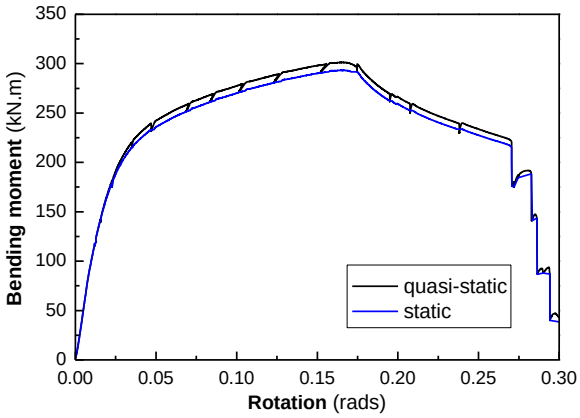

Fig. 4. Example of converting original curve to static curve

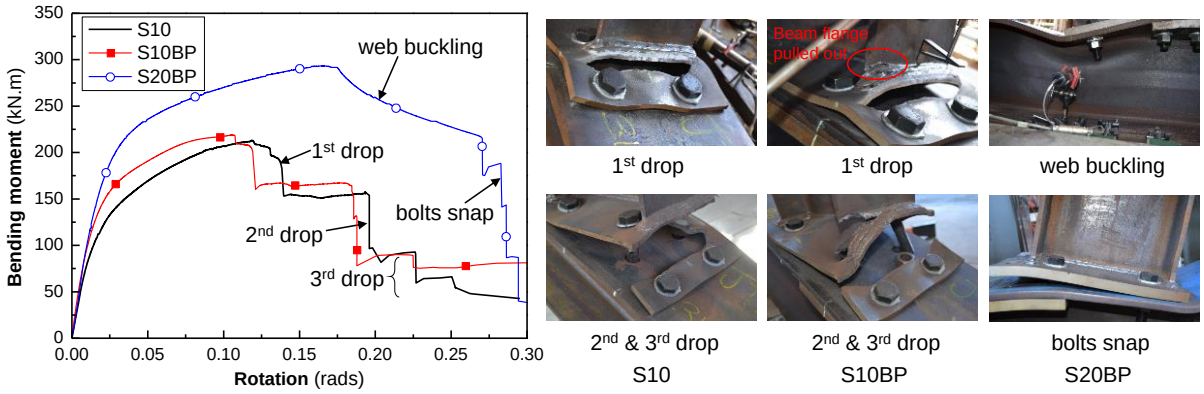

Fig. 5. Results of the major-axis bending tests

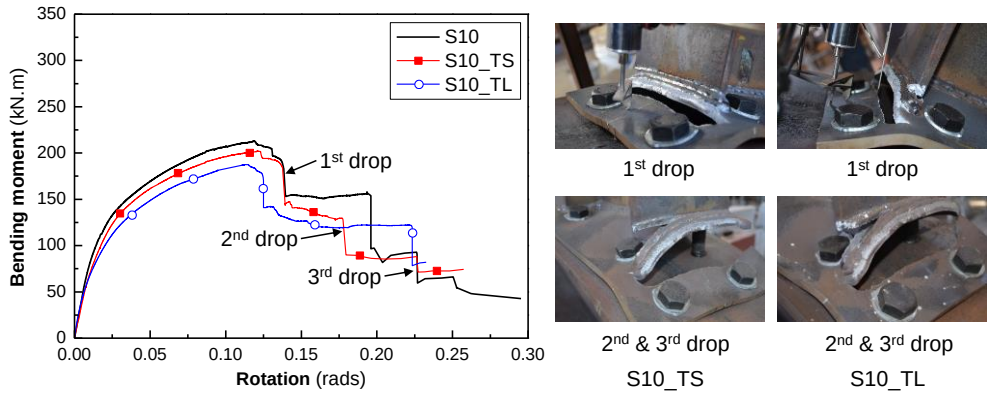

507

508 Fig. 6. Results of the combined bending and tension tests on the 10-mm-thick end-plate connections

509

510

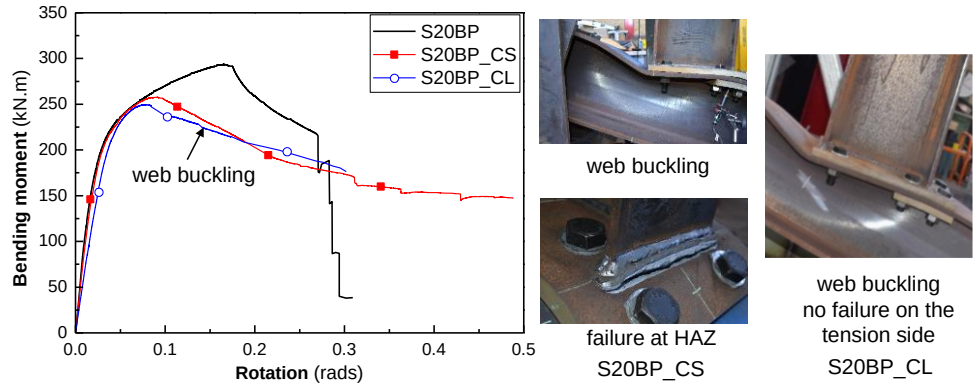

511

512 Fig. 7. Results of the combined bending and compression tests of the 20-mm-thick end-plate connections

513

514

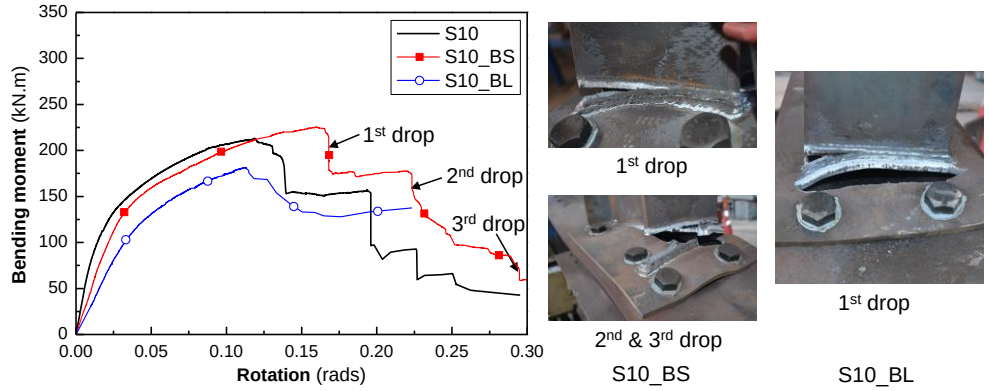

515

516 Fig. 8. Results of the bi-axial bending tests on the 10 mm thick end-plate connections

517

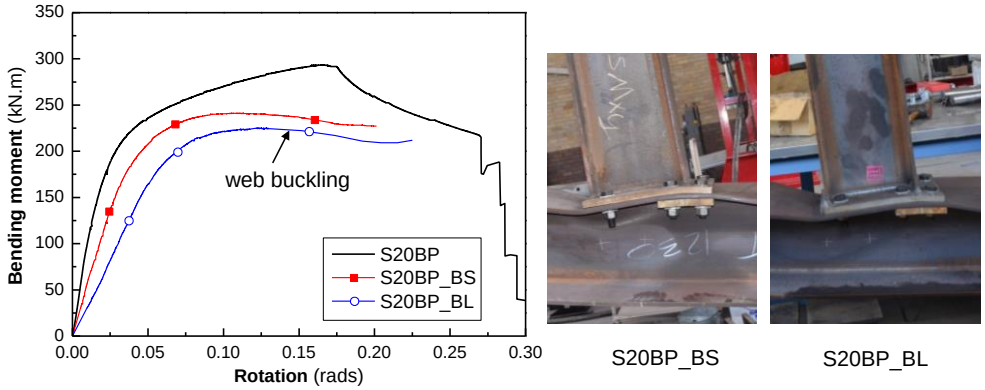

Fig. 9. Results of the bi-axial bending tests on the 20 mm thick end-plate connections

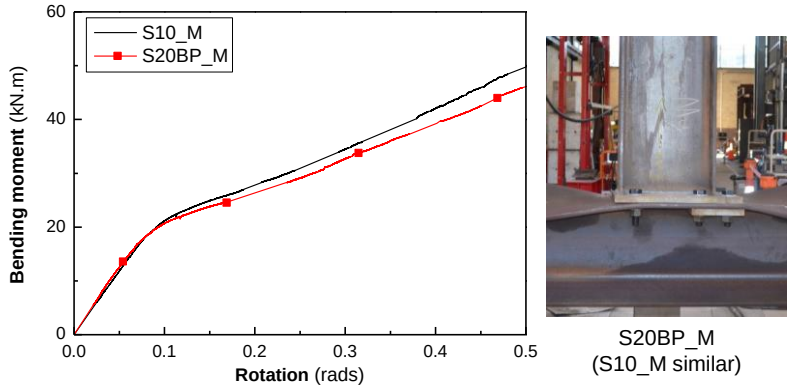

Fig. 10. Results of the minor-axis bending tests

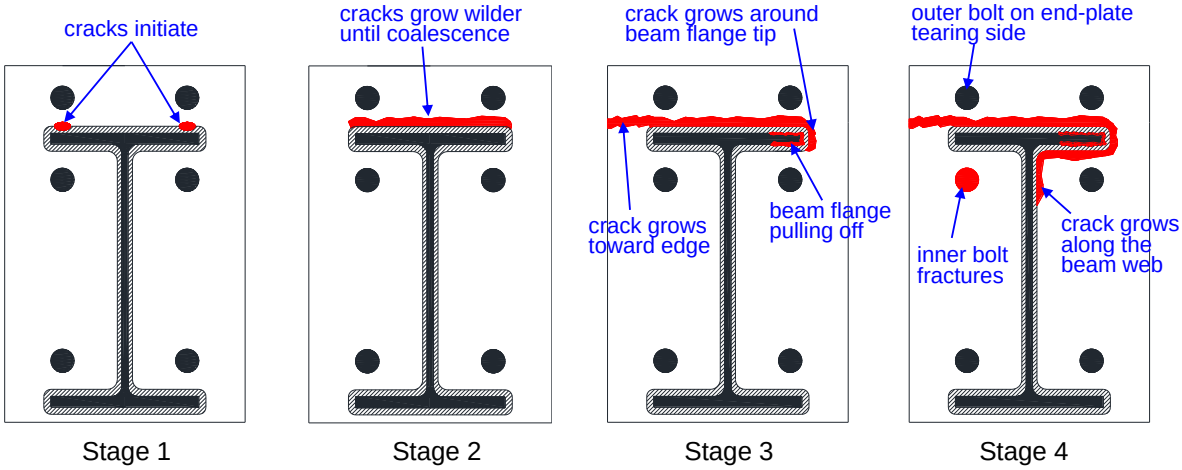

Fig. 11. Failure mechanism for end-plate bending failure mode

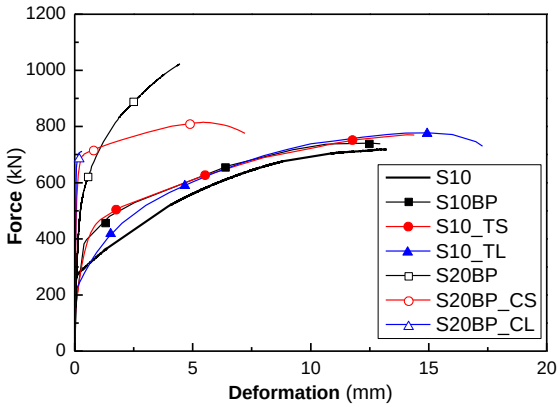

528

529 Fig. 12 Force versus displacement responses of the end-plate bending component.

530

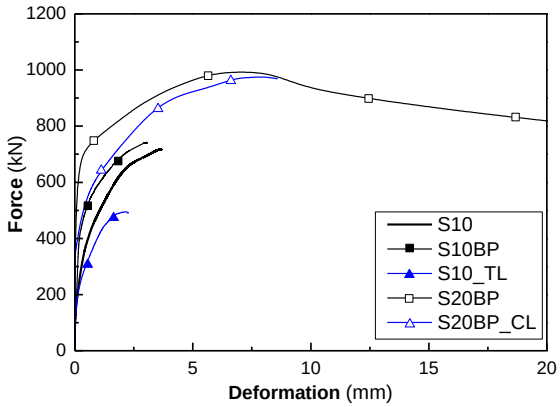

531

532 Fig. 13 Force versus displacement responses of the column web buckling component.

533

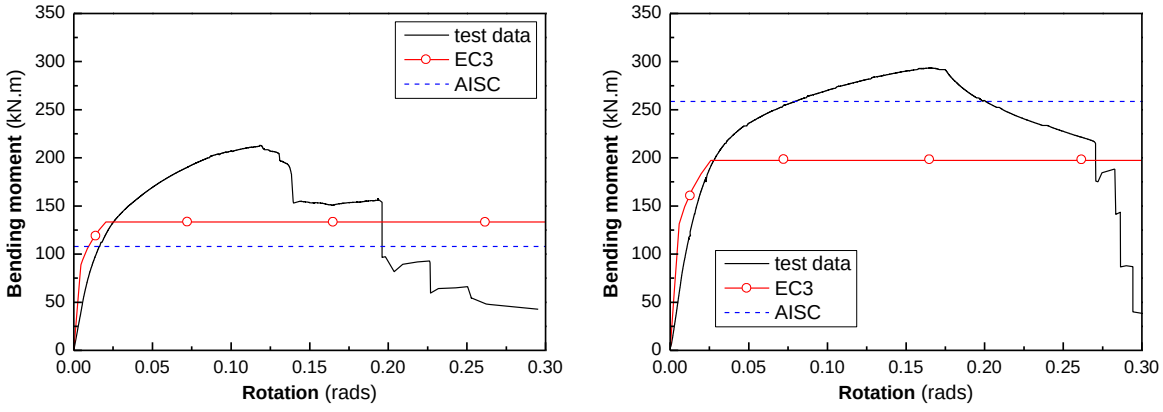

534

535 (a) S10 (b) S20BP

536 Fig.14 Connection assessment according to Eurocode3 and AISC Design Guide.

537